PHILOSOPHICAL TRANSACTIONS OF THE ROYAL SOCIETY B BIOLOGICAL SCIENCES

Extracellular Current Flow and Potential during Quantal Transmission from Varicosities in a Smooth Muscle Syncytium

M. R. Bennett, W. G. Gibson and R. R. Poznanski

Phil. Trans. R. Soc. Lond. B 1993 **342**, 89-99
doi: 10.1098/rstb.1993.0140

Extracellular current flow and potential during quantal transmission from varicosities in a smooth muscle syncytium

M. R. BENNETT, W. G. GIBSON AND R. R. POZNANSKI

The Neurobiology Research Centre, Department of Physiology and The School of Mathematics and Statistics, University of Sydney, New South Wales 2006, Australia

CONTENTS

SUMMARY

A discrete model has been developed that describes the extracellular current that flows in a smooth muscle syncytium upon the secretion of a quantum of transmitter onto a smooth muscle cell in the syncytium. This allows a description to be given of the current (called the excitatory junctional current (EJC)) recorded by an electrode of given diameter placed on the surface of the muscle, during synaptic transmission from a varicosity situated anywhere in the muscle. The EJC is of maximum negative amplitude when the varicosity is at the surface of the muscle near the inside rim of the electrode and decreases as the varicosity moves to the centre of the electrode. It is of maximum positive amplitude when the varicosity is at the surface near the outside rim of the electrode and declines rapidly in amplitude as the varicosity is removed further from the outside rim. Smaller diameter electrodes give larger EJCs than larger diameter electrodes for most positions of the varicosity on the surface of the muscle. The EJC amplitude declines for varicosities beneath the electrode that are not on the surface of the muscle, but deep in the tissue. The rate of this decline is greater the smaller the diameter of the electrode.

The timecourse of the EJC is largely invariant under changes in the position of the varicosity with respect to the recording electrode. Changes in the polarity of the current flow during a single EJC can occur, however, if two varicosities secrete transmitter simultaneously, one inside the electrode and one outside, and the timecourse of the currents due to the individual varicosities is either the same or slightly different.

This theoretical work has been used to interpret a number of recent experimental studies of extracellular current flow during autonomic neuromuscular transmission.

Phil. Trans. R. Soc. Lond. B (1993) **342**, 89–99
Printed in Great Britain

1. INTRODUCTION

The release of transmitter from sympathetic nerve terminals gives rise to excitatory junction potentials (EJPs) across the smooth muscle membrane which can be recorded with an intracellular electrode (Burnstock & Holman 1962). The discovery that these EJPs did not reverse polarity on depolarization due to current injection from an intracellular electrode (Bennett & Merrillees 1966) led to the realization that synaptic transmission from autonomic nerve varicosities had to be considered in the context of current flow in an electrical syncytium. Such a syncytium arises because of the electrical coupling between individual smooth muscle cells (Bennett 1967; Tomita 1970). The introduction of a discrete model for the three-dimensional smooth muscle syncytium (Bennett 1972, 1973) provided a scheme of considerable generality, as the geometry and peripheral termination of the array of elements representing the smooth muscle cells could be varied according to requirements. This model has been used to investigate the electrical spread of current within the smooth muscle syncytium for both spontaneous quantal release of transmitter from individual varicosities and for the evoked release of transmitter from many varicosities (Bennett 1972; Purves 1976).

The analysis of the electrical signs of transmitter release onto smooth muscle cells has recently been extended by the introduction of techniques for recording potential changes due to the extracellular current flow that accompanies the action of a quantum of transmitter (Brock & Cunnane 1987). In this case, an extracellular electrode, typically of about 50 μm diameter, is lowered onto the surface of a smooth muscle and negative pressure applied to the inside of the pipette (Brock & Cunnane 1988). By this means, mostly negative-going excitatory junctional currents (EJCs) are recorded, due to either spontaneous or evoked secretion of transmitter quanta. They are attributed to transmitter secretion from varicosities 'within' the pipette (Stjärne & Stjärne 1989). The EJCs typically have a skewed amplitude–frequency distribution, with the very large number of smaller EJCs disappearing into the noise level of about 10 μV (Åstrand & Stjärne 1988). These skewed distributions have been variously attributed to several different causes: the distances between varicosities and smooth muscle cells varies so that varicosities some distance from the muscle will give rise to small EJCs (but see Hirst & Neild (1980) for arguments showing more normal distributions of amplitudes due to spontaneous secretions); then again, there may be variations in the density of receptors beneath the varicosities; finally, it has been suggested that the size of the quantum of transmitter in a vesicle may vary greatly (Åstrand *et al.* 1988). More recently, a new approach to the analysis of the electrical signs of transmitter release has been developed that involves recordings being made with small-diameter ($\approx$4 μm) extracellular pipettes placed over one or two visualized sympathetic-nerve varicosities, without the introduction of any negative pressure to the inside of the pipette (Lavidis & Bennett 1992). This type of recording of exclusively negative-going EJCs gives rise to amplitude–frequency distributions that are both normal and skewed.

Previous discrete models of current flow and potential in the three-dimensional syncytium of smooth muscle (Tomita 1970; Bennett 1972; Purves 1976) are not adequate to describe current flow and potential in the extracellular space, as they treat the interstitial milieu as being at earth potential. These models, therefore, do not allow predictions to be made concerning the potential drop in the extracellular space around the muscle, or in the interstitial space between the muscle cells in the syncytium, during secretion from varicosities at a known site in the syncytium. As a consequence, it is not known how the spatial and temporal distribution of the current flow recorded with an extracellular electrode on the surface of the smooth muscle during synaptic transmission is to be interpreted. It is the aim of this paper to provide a discrete model of the smooth muscle syncytium that will allow for such interpretations.

2. A MODEL FOR EXTRACELLULAR CURRENT FLOW AND POTENTIAL DURING SYNAPTIC TRANSMISSION IN A SYNCYTIUM

(*a*) *A discrete bidomain model of a muscle syncytium*

Previously (Bennett 1972, 1973; Purves 1976), the smooth muscle bundle has been modelled as a three-dimensional rectangular grid, the nodes representing the muscle cells and the joining lines representing the intracellular resistances. To include the interstitial medium, it is necessary to extend this to a bidomain model, in which there are now two grid systems, one representing the intracellular region and the other the interstitial region. These two grids occupy the same region of space, and are connected at every node by an *RC* circuit representing the membrane of a muscle cell (figure 1).

(*b*) *Equations for the intracellular and interstitial potentials*

The muscle tissue occupies the region $z \leqslant 0$, and the nodes of the grid are labelled by the rectangular cartesian coordinates (i, j, k), where i, j, k take integer values with $-\infty < i < \infty$, $-\infty < j < \infty$, $-\infty < k \leqslant 0$. Let V^i_{ijk} denote the deviation of the intracellular potential at node (i, j, k) from its resting value; that is, $V^i_{ijk} = \bar{V}^i_{ijk} - E_m$ where $\bar{V}^i_{ijk}$ is the true intracellular potential and E_m is the resting potential. Let V^e_{ijk} denote the interstitial potential at node (i, j, k), and let I_{ijk} be the corresponding membrane current; that is, I_{ijk} is the current flowing from the intracellular to the interstitial space at node (i, j, k) (figure 2*a*).

Conservation of intracellular current at node (i, j, k) gives

$$I_{ijk} + (1/R_i)\,(6V^i_{ijk} - \Sigma' V^i_{lmn}) = 0, \quad (1)$$

where Σ' denotes a sum over the six nodes (l, m, n) which are the nearest neighbours of (i, j, k), and R_i is the resistance between two intracellular nodes. For the present, R_i is taken to be isotropic; the extension to the case where it can take different values in the x, y and z directions will be given below. Similarly, conservation of the interstitial current at node (i, j, k) gives

$$-I_{ijk} + (1/R_e)\,(6V^e_{ijk} - \Sigma' V^e_{lmn}) = 0, \quad (2)$$

where R_e is now the interstitial resistance, again for the present taken to be isotropic. Adding equations (1) and (2) gives

$$6V^+_{ijk} - \Sigma' V^+_{lmn} = 0, \quad (3)$$

where V^+_{ijk} is an auxiliary potential function defined by

$$V^+_{ijk} = V^i_{ijk} + (1/\kappa)V^e_{ijk}, \quad (4)$$

and $\kappa = R_e/R_i$. Also, from equations (1) and (2),

$$(R_i + R_e)I_{ijk} + 6V_{ijk} - \Sigma' V_{lmn} = 0, \quad (5)$$

where V_{ijk} is the membrane potential defined by

$$V_{ijk} = V^i_{ijk} - V^e_{ijk}. \quad (6)$$

(More precisely, V_{ijk} is the deviation of the membrane potential from its resting value, but for brevity it will be referred to as the membrane potential.)

The transmembrane coupling between the intracellular and interstitial mediums at each node is represented by an RC circuit, with resistance, R_m and capacitance C_m, these values being the same for all nodes (figure 2*a*). The spontaneous junction potential is located at node (p, q, r), and its action is simulated by a variable conductance change $g(t)$ in series with a constant driving potential of magnitude E_0. Thus at node (p, q, r) the basic RC circuit is altered, as shown in figure 2*b*. The membrane current at any node (i, j, k) is therefore

$$I_{ijk} = C_m(\partial V_{ijk}/\partial t) + (1/R_m)V_{ijk} + (V_{ijk} - E_0)g(t)\delta_{(ijk)(pqr)}, \quad (7)$$

where $\delta_{(ijk),(pqr)} = 1$ if $(i, j, k) \equiv (p, q, r)$, and is zero otherwise. Using equation (7) to substitute for the membrane current in equation (5), and making the change of variable $T = t/\tau_m$, where $\tau_m = R_mC_m$, gives

$$(dV_{ijk}/dT) + V_{ijk} = \Lambda^2(\Sigma' V_{lmn} - 6V_{ijk}) - R_m(V_{ijk} - E_0)g(T)\delta_{(ijk)(pqr)}, \quad (8)$$

where $\Lambda = \sqrt{[R_m/(R_i + R_e)]}$ and $g(T)$ is the conductance change in terms of the scaled time T. In the numerical calculations, $g(T)$ is taken to be an α-function (Jack & Redman 1971; Purves 1976):

$$g(T) = g_0\alpha T e^{1-\alpha T}, \quad (9)$$

where g_0 and α are constants, but the rest of this section does not depend on the specific choice of $g(T)$.

The advantage of changing to the potentials V^+_{ijk} and V_{ijk} is that they satisfy the uncoupled equations (3) and (8). Once these are solved, the original potentials can be found from

$$V^i_{ijk} = [1/(1 + \kappa)]\,(\kappa V^+_{ijk} + V_{ijk}), \quad (10)$$

$$V^e_{ijk} = [\kappa/(1 + \kappa)]\,(V^+_{ijk} - V_{ijk}). \quad (11)$$

The extension to the anisotropic case is made by replacing the scalar resistances R_i and R_e by the vectors $R_i = (R_{ix}, R_{iy}, R_{iz})$ and $R_e = (R_{ex}, R_{ey}, r_{ez})$. The above analysis proceeds almost unchanged, provided the anisotropy is assumed to be identical for both intracellular and interstitial regions; that is,

$$R_{ex}/R_{ix} = R_{ey}/R_{iy} = R_{ez}/R_{iz} = \kappa. \quad (12)$$

The potentials V^i_{ijk} and V^e_{ijk} are still given by equations (10) and (11), and V^+_{ijk} still satisfies equation (3), which can be written explicitly as

$$6V^+_{ijk} - (V^+_{i+1jk} + V^+_{i-1jk} + V^+_{ij+1k} + V^+_{ij-1k} + V^+_{ijk-1} + V^+_{ijk+1}) = 0. \quad (13)$$

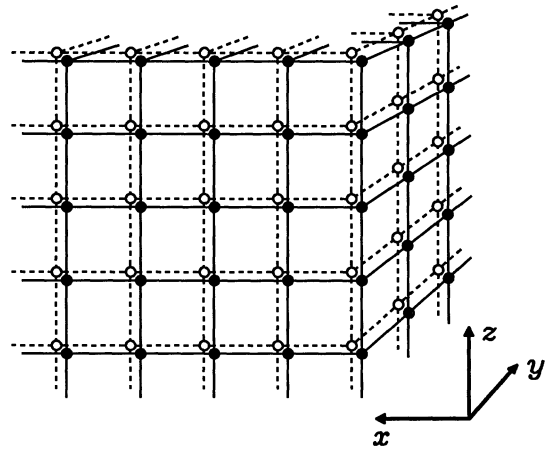

Figure 1. Diagram of a discrete bidomain model for the three-dimensional smooth muscle syncytium. The x- and z-axes are in the transverse plane of the muscle and the y-axis is along the longitudinal axis of the muscle. Each filled node represents a point within a single smooth muscle cell, coupled to six other cells; the coupling is represented by continuous lines, the inside of each cell being coupled to the inside of four other cells in the transverse plane and to two other cells in the longitudinal direction; each of these lines represents the resistance of the intracellular pathway between adjacent cells. Each open node represents a point lying just outside a single smooth muscle cell, coupled to similar points outside six other cells in the same configuration as that for the inside points; these are represented by discontinuous lines, each of which represents the resistance of the interstitial pathway between adjacent cells. The resistance of the intracellular and interstitial pathways is not necessarily the same in the x-, y- and z-directions. Each of the intracellular nodes is coupled to an adjacent interstitial node by the parallel resistance and capacitance of the cell membrane. The figure shows the general structure of the discrete model (compare with figure 23 in Bennett (1972)). Note that only a few nodes and their connections have been drawn. Theoretically, the system is infinite in the x- and y-directions and semi-infinite in the z-direction, with the muscle tissue occupying the region $z < 0$. In a practical calculation, it is sufficient to take a maximum of 30 nodes in each of the x- and y-directions and 15 in the z-direction.

PHILOSOPHICAL TRANSACTIONS OF THE ROYAL SOCIETY B BIOLOGICAL SCIENCES

The membrane potential satisifes a modification of equation (8):

$$dV_{ijk}/dT + V_{ijk} = \Lambda_x^2(V_{i+1jk} + V_{i-1jk} - 2V_{ijk}) + \Lambda_y^2(V_{ij+1k} + V_{ij-1k} - 2V_{ijk}) + \Lambda_z^2(V_{ijk+1} + V_{ijk-1} - 2V_{ijk}) - R_m(V_{ijk} - E_0)g(T)\delta_{(ijk)(pqr)}, \quad (14)$$

where $\Lambda_x = \sqrt{[R_m/(R_{ix} + R_{ex})]}$, etc.

(*c*) *Boundary conditions on the intracellular and interstitial potentials*

It is assumed that initially there is no electrical activity in the muscle tissue. Thus

$$V^i_{ijk} = 0,\ V^e_{ijk} = 0, \text{ for all } i,j,k \text{ when } T = 0. \quad (15)$$

Because the only disturbance to the system comes from the junction potential, at a sufficient distance from (p, q, r) the potentials must remain at zero; that is,

$$V^i_{ijk},\ V^e_{ijk} \to 0 \quad \text{as} \quad |i|, |j| \to \infty, \quad k \to -\infty. \quad (16)$$

It remains to establish the boundary conditions on the surface $z = 0$. Because the muscle tissue does not intrude into the region $z > 0$, it follows that the z-component of the intracellular current must vanish for $z > 0$. In terms of the discrete model, this is formulated as

$$V^i_{ij1} = V^i_{ij0}, \quad \text{for all} \quad i,j. \quad (17)$$

At the muscle surface, interstitial space becomes extracellular space and the interstitial current will flow into the region $z > 0$. However, in the present case of a spontaneous junction potential all the current eventually returns to the node (p, q, r). The assumption is made that the interstitial current may penetrate some distance into the extracellular region, but that the main contribution to the EJC will come from current flowing across the circumference of the electrode in the xy-plane. Thus, to a first approximation, the z-component of extracellular current is neglected. (A more detailed treatment of this surface layer is the subject of further investigation.) Thus the boundary condition for V^e_{ijk} is also taken to be

$$V^e_{ij1} = V^e_{ij0}, \quad \text{for all} \quad i,j. \quad (18)$$

From equations (4) and (6) it is clear that V^+_{ijk} and V_{ijk} satisfy the same initial condition and boundary conditions as V^i_{ijk} and V^e_{ijk}.

(*d*) *The method of solving the equations for the intracellular and interstitial potentials*

From equation (13) and the boundary conditions specified in the previous section, the only solution for the auxiliary potential V^+_{ijk} is

$$V^+_{ijk} = 0, \quad \text{for all} \quad i,j,k. \quad (19)$$

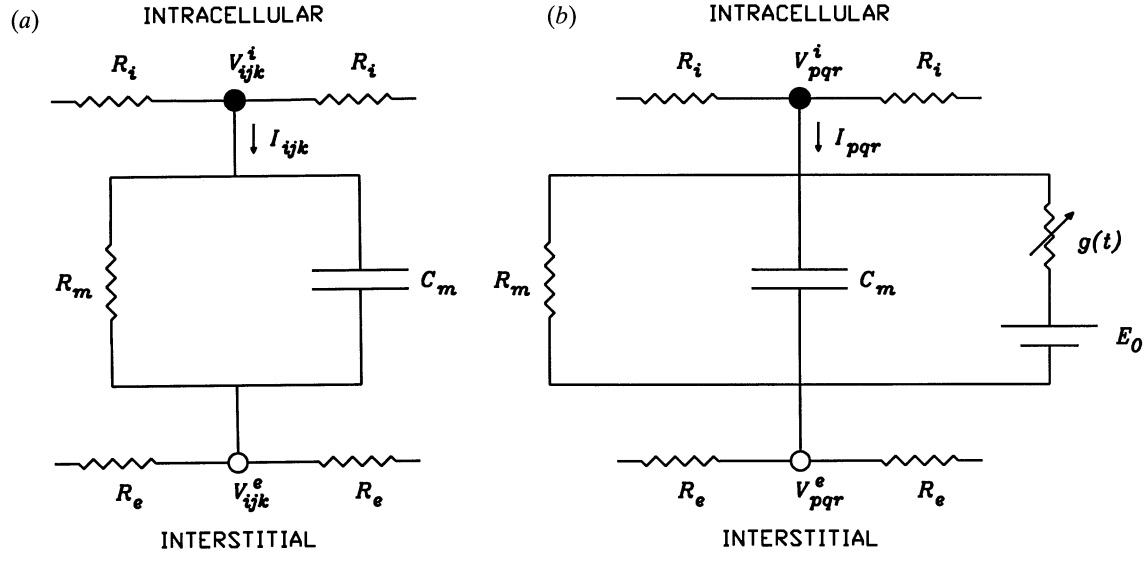

Figure 2. (*a*) Equivalent circuit for the transmembrane connection between an intracellular and an interstitial node. This circuit connects each filled node in figure 1 to its adjacent open node. R_m and C_m are the membrane resistance and capacitance, I_{ijk} is the membrane current, V^i_{ijk} is the deviation of the intracellular potential from its resting value, V^e_{ijk} is the interstitial potential, and R_i and R_e are the intracellular and interstitial resistances. Only the one-dimensional case is illustrated; in the three-dimensional case there will be six such resistances at each node, possibly taking different values in the x-, y- and z-directions. (*b*) Equivalent circuit for a spontaneous junction potential. At sites where there is spontaneous transmitter release, the circuit (*a*) is modified by the addition of a reversal potential E_0 and a variable conductance $g(t)$.

PHILOSOPHICAL TRANSACTIONS OF THE ROYAL SOCIETY B BIOLOGICAL SCIENCES

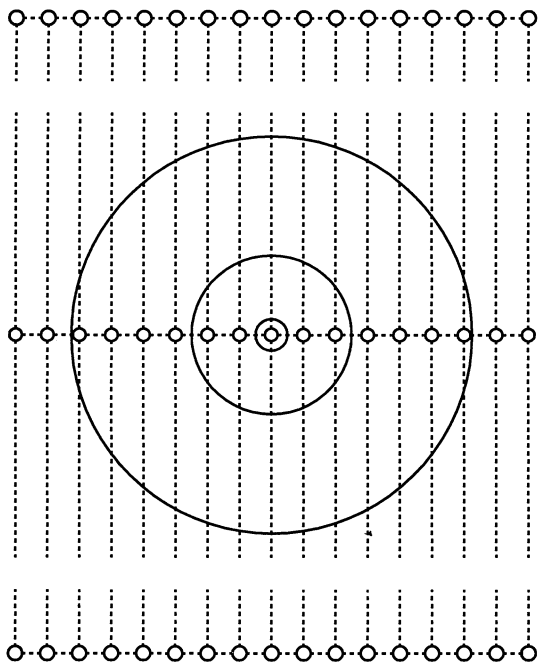

Figure 3. The grid of broken lines represents the interstitial coupling of the muscle cells at the surface ($z=0$), the internodal distance being 4 μm in both the x- and z-directions, and in the order of 100 μm in the y-direction, reflecting the spatial dimensions of smooth muscle cells. The circles show the placement of the tips of three electrodes, of diameters 4 μm, 20 μm and 50 μm. The total current flowing across the tip of an electrode is found by adding the individual currents in the internodal grid lines crossing the circumference of the electrode. (In figure 1, for simplicity, the grid was shown as rectangular; to correspond with this figure, it should be stretched in the y-direction. Alternatively, the grid could be left as rectangular and the circular electrodes could be replaced by ones of elliptical cross-section.)

Thus, from equations (10) and (11), the intracellular and interstitial potentials are both simply proportional to the membrane potential; in particular, the interstitial potential is

$$V^e_{ijk} = -[\kappa/(1+\kappa)]V_{ijk}. \quad (20)$$

The problem then is to solve equation (14) for the membrane potential V_{ijk} under the boundary conditions specified in the previous section, namely

$$V_{ijk} = 0, \quad \text{for all} \quad i,j,k \quad \text{when} \quad T = 0, \quad (21)$$

and

$$V_{ij1} = V_{ij0}, \quad \text{for all} \quad i,j. \quad (22)$$

Equation (14) is a combination of a difference equation in the spatial variables and a differential equation in time. The standard method of solution is to replace the time derivative by a finite difference, and then to solve the resulting set of equations by some implicit method. This has the disadvantage of requiring the solution of a set of equations, and can be both cumbersome to program and slow to run. In the present calculation, a combination of a finite difference scheme centred in time and a method of updating on a staggered mesh (Roberts & Weiss 1965) has been used; this gives a stable explicit method which is straightforward to program and fast in execution.

(*e*) *The calculation of the extracellular current measured by an electrode*

The remaining part of the calculation involves using the potentials V^e_{ijk} to find the total current flowing across the tip of an electrode. This is done simply by forming the algebraic sum of all the currents flowing in the interstitial resistances which cross the edge of the electrode. It is assumed that the electrode tip is of circular cross section of diameter D and is symmetrically placed with respect to the grid. Without loss of generality, the centre of the circular tip can be placed at the point (0, 0, 0), and figure 3 shows this configuration for tips of diameters $D = 4$ μm, 20 μm and 50 μm.

The total electrode current is given by

$$I_{\text{electrode}} = \Sigma\,(\Delta V^e/R_{\text{grid}}), \quad (23)$$

where ΔV^e is the difference in the interstitial potential between two contiguous nodes in the $z = 0$ plane and the sum is over all grid lines cut by the circumference of the electrode tip. The sign of ΔV^e is chosen so that the positive direction of current flow is across the circumference of the tip from inside to outside. Thus a positive value for $I_{\text{electrode}}$ indicates a net flow of current out across the circumference of the electrode tip; a negative value indicates a net flow of current in across the electrode tip. The boundary conditions at the electrode tip are more complex than this and are at present under investigation.

3. RESULTS

The recent experimental observations dealing with the extracellular current flow associated with transmitter secretion in a smooth muscle syncytium require interpretation in terms of a sound theoretical model. For example, how does the position of the extracellular recording electrode with respect to the site of transmitter secretion determine the polarity of the EJC? Are the amplitude–frequency distributions of EJCs, recorded with an electrode that has negative pressure, skewed because of the spatial decrement in the syncytium of currents generated at a site? The present section will attempt to investigate these questions concerning the polarity of EJCs and their amplitude distribution.

(*a*) *Numerical values for the parameters*

The numerical values of the parameters used in the calculations are listed in table 1. The classical method for determining the resistance properties of a bidomain was pioneered for the heart by Clerc (1975). He used both the time constant of the exponential rise in potential at the foot of the propagating action potential (Hodgkin 1954) and the voltage gradient near the

Table 1. *Values of the parameters used in the numerical calculations*

(The last three quantities are defined in terms of the earlier ones, so their numerical values follow from the ones already assigned. The assumed grid spacings are 4 μm in the *x*- and *z*-directions and 140 μm in the *y*-direction.)

quantity	symbol	value	reference
membrane resistance	R_m	$3.6 \times 10^9\ \Omega$	Bennett (1973)
membrane capacitance	C_m	$5.6 \times 10^{-11}\ F$	(see text)
intracellular resistance	R_i	$(14, 1750, 14) \times 10^6\ \Omega$	(see text)
extracellular resistance	R_e	$(3.5, 437.5, 3.5) \times 10^6\ \Omega$	(see text)
conductance rate constant	α	14	(see text)
peak conductance	g_0	$3.45 \times 10^{-8}\ \Omega^{-1}$	(see text)
driving potential	E_0	5×10^{-2} V	Purves (1976)
space constant	Λ	(14.34, 1.28, 14.34)	(follows)
membrane time constant	τ_m	0.2 s	(follows)
anisotropy ratio	κ	0.25	(follows)

middle of a trabecular bundle to subthreshold steps of current to determine the resistance properties. The approach allowed estimates to be made of the ratio of the intracellular to interstitial longitudinal resistivity, the ratio of the intracellular to interstitial transverse resistivity, the ratio of intracellular transverse to intracellular longitudinal resistivity, and the ratio of interstitial transverse to interstitial longitudinal resistivity. Experiments have not yet been done on smooth muscle which will allow estimates of these ratios, but they are now in progress. In the present work the resistances are based on the resistivity ratios determined for heart muscle, with the exception that the external resistances have been adjusted so as to maintain equal anisotropy.

Cunnane & Manchanda (1990) give a value of 210 ms for the membrane time constant τ_m, and this has been rounded to 200 ms in table 1. It is then necessary to assign the value 5.6×10^{-11} F to C_m, which can be compared with the value 2.8×10^{-11} F of Bennett (1973). Cunnane & Manchanda (1990) also give a value for the rate constant α of 11.5, but this is based on measurements of an averaged EJC representing the summed membrane current arising from the action of transmitter released from several nerve fibres. Results quoted for the timecourse of EJCs resulting from the spontaneous release of transmitter from a single site show an earlier peak and a shorter time constant of decay, making the choice $\alpha = 14$ more appropriate. The value for g_0 is chosen to give a peak potential of 10 mV in an infinite monodomain (cf. Purves 1976).

Figure 4 shows the results of a typical calculation using the above parameter values. Transmitter release occurs at a varicosity situated on the muscle surface at the origin. The calculated membrane potential is shown at the origin and also at a distance of two nodes away in the *x*-direction. The EJC is measured by using a surface electrode of diameter 20 μm centred on the origin (see § 3(*b*) for more details).

Note that the timecourses of all three curves are almost the same, and in particular that the decay times of the membrane potentials and of the EJC are much shorter than the membrane time constant of 200 ms. This shows that, in the case of only a single varicosity, the governing factor is the timecourse of transmitter action. The other extreme would be the isopotential case (where the whole syncytium acquires the same membrane potential), corresponding to many releases, in which case the decay times of the membrane potential and of the EJC are governed by the membrane time constant. (The difference between these two situations for the monodomain case has been discussed by Bennett (1972) and Purves (1976).)

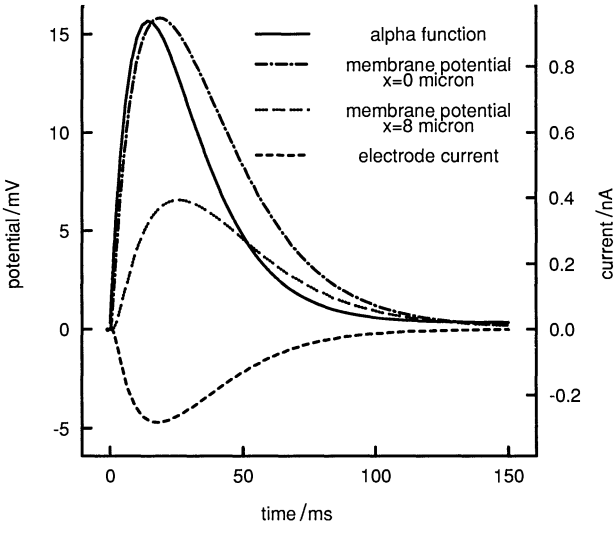

Figure 4. The calculated membrane potential and the excitatory junction current (EJC) resulting from the release of transmitter from a varicosity situated at the origin. The parameter values are as given in table 1. The timecourse of the α-function describing the conductance change is shown as a solid line (no amplitude scale is shown, but its peak corresponds to a conductance of 34.5 nS). Two membrane potentials are shown, one measured at the origin and the other at a distance of two nodes in the *x*-direction ($x = 8$ μm). The EJC is measured by a surface electrode of diameter 20 μm centred on the origin.

(*b*) *Changes in excitatory junctional currents for secretion at different sites on the surface of the muscle syncytium*

Different-size glass microelectrodes, with tip diameters in the range 4–50 μm, are used to record the extracellular signs of synaptic transmission from varicosities in smooth muscle. The extracellular current, referred to as the excitatory junctional current (EJC), is recorded from the surface of the muscle, sometimes after introducing a slight negative pressure to the

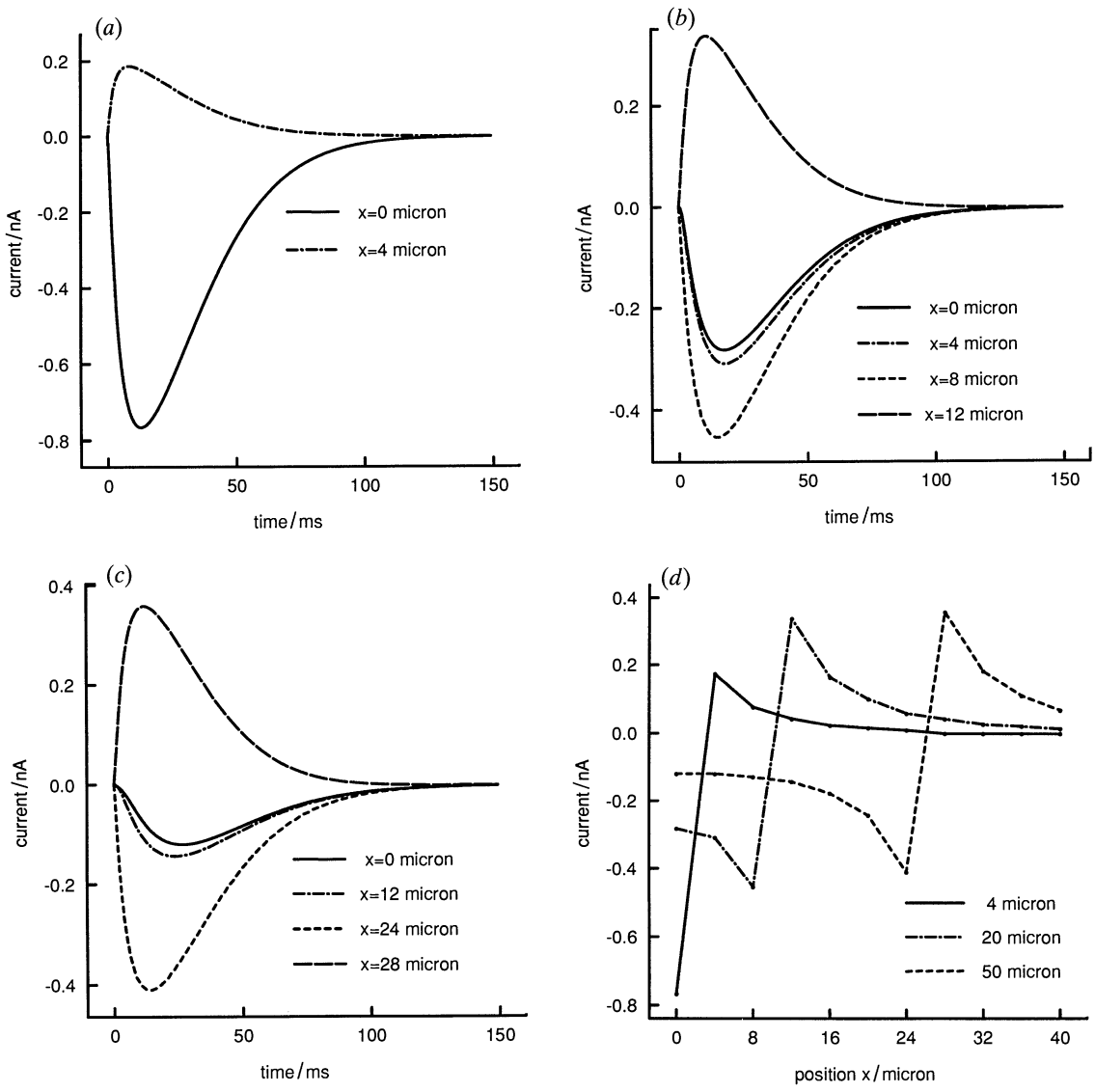

Figure 5. Changes in the amplitude and polarity of the EJCs when the transmitter secretion occurs from varicosities on the surface of the muscle ($z=0$) at different distances along the x-axis from the centre of the extracellular recording electrode. The centre of the electrode is positioned at (0, 0, 0) and the varicosity is positioned at (x, 0, 0). (*a*) Recordings with a 4 μm diameter electrode. The solid line is for a varicosity at the centre of the electrode, and the broken line is for $x=4$ μm, which is at the closest node outside the electrode. In the latter case the EJC has reversed polarity with a much reduced amplitude. (*b*) Recordings with a 20 μm diameter electrode. Note the increase in peak negative amplitude of the EJC as the secreting varicosity moves from $x=0$ towards the inner edge of the electrode, and the now more pronounced reversal of polarity as it passes beyond this edge. (*c*) Recordings with a 50 μm diameter electrode. The amplitude due to a varicosity near the inner edge of the electrode is now much greater than that due to one at the centre. (*d*) Changes in the peak amplitude of the EJC as the surface varicosity moves out along the x-axis, for 4 μm, 20 μm and 50 μm electrodes. The curves show clearly the increase in EJC amplitude as the varicosity approaches the inside edge of an electrode and the polarity reversal as it passes outside.

electrodes so as to produce a seal with the muscle of resistance less than 1 MΩ. The EJC recorded in this way is typically about 0.2 nA when a patch-clamp recording is made with a 50 μm diameter electrode, or about 40 μV when a conventional recording is made with an electrometer. The use of the dye D_iOC_2 (5) to fluoresce varicosities on the surface of a smooth muscle allows recordings to be made of the secretory activity of selected sets of varicosities (Lavidis & Bennett 1992).

The first question to be asked about this procedure is what are the expected amplitudes and polarities of the EJCs due to surface varicosities, when recorded in this way with different diameter external electrodes? Figure 5 shows the results obtained by evaluating equation (23) for the extracellular current generated by transmitter release from surface varicosities at different distances along the x-axis from the centre of different diameter electrodes. Three clear points emerge: first, no matter what the diameter of the electrode, from 4 μm (figure 5*a*) to 50 μm (figure 5*c*), or the position of the transmitter source, the overall timecourse of the EJC remains almost the same, decreasing to near zero in about 100 ms (see also

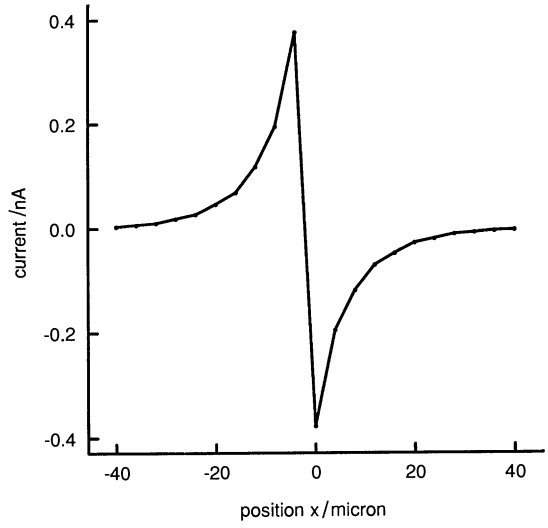

Figure 6. The current flow in the grid lines lying along the *x*-axis on the muscle surface, when the varicosity is at the origin. The direction of current flow is always towards the origin, becoming very large close to the varicosity. This graph can be used to interpret the magnitude and sign of the EJC for different positions of the varicosity relative to the edge of different-sized electrodes.

Cunnane & Manchanda 1990); second, the maximum amplitude EJC is recorded with the smaller-diameter electrodes (cf. figure 5*a*,*b*,*c*); third, the EJC changes polarity when the varicosity is just outside the recording electrode.

The EJC increases in size as the varicosity is displaced further from the centre of the electrode (figure 5*a*,*c*). This is shown clearly in figure 5*d*, where for the 20 μm and 50 μm electrodes the peak amplitude of the EJC increases in size as the varicosity moves from the centre to the inside periphery of the electrode, this increase being a trebling in the case of the 50 μm electrode. (In the case of the 4 μm electrode, the present discrete model only allows one position for a surface varicosity inside the electrode, so this effect cannot be investigated.) Note also that there is a change in the initial timecourse of the EJC, depending on the position of the varicosity inside the electrode. This again is particularly noticeable in the case of the 50 μm electrode (figure 5*c*) when the EJC due to a varicosity at the centre of the electrode ($x = 0$ μm) exhibits a much slower initial decrease than the one just inside the circumference ($x = 24$ μm). This can be explained by the fact that initially the current flow is confined to a region very close to the varicosity, and takes a finite time to spread to the circumference of the electrode.

The polarity reversal as a varicosity moves outside the electrode is very pronounced for the larger electrodes (figure 5*b*,*c*); the effect is so great that the EJC due to a surface varicosity just outside the electrode rim is comparable with that of one just inside the rim and can dominate those due to varicosities at more interior positions. Thus the simultaneous release of transmitter at several varicosities could result in a positive-going EJC, even if one or more of them were within the electrode tip. (When the varicosities are at different positions, interference effects are small, and for a good approximation one can simply add the resulting individual EJCs.)

The reason for a number of the above effects can be seen from a consideration of the extracellular current flow generated near the varicosity during transmission. Figure 6 shows the current flow in the grid lines lying along the *x*-axis on the muscle surface, when the varicosity is at the origin. The direction of current flow is always towards the origin, becoming very large close to the varicosity. If the varicosity is at the centre of a 20 μm or 50 μm electrode, the current flow across the circumference is of moderate magnitude, and so a medium-amplitude EJC results. As the varicosity approaches the inside rim of the electrode, part of its circumference crosses a grid line carrying a large current, and the amplitude of the EJC increases. As the varicosity passes outside the rim, the electrode circumference still cuts a line of intense current, but the current is in the opposite direction, so the polarity of the EJC reverses.

(*c*) *Changes in excitatory junctional currents for secretion at different sites in the depth of the muscle syncytium*

Figure 7 shows the extracellular current flow, as calculated using equation (23), generated by transmitter release from varicosities at successively greater depths into the syncytium beneath the recording electrode, for different-size electrodes. Again, the timecourse of the EJC remains almost the same, regardless of the depth of the varicosity or the recording electrode used (figure 7); maximum-amplitude EJC is still recorded with the smaller diameter electrodes (cf. figure 7*a*,*b*,*c*); furthermore, there is no change in polarity of the EJC. The most important point that emerges is that, for the smaller diameter electrodes, the maximum size of the EJC declines rapidly with varicosities at increasing depths in the syncytium (figure 7*d*). For a 4 μm electrode, the EJC generated by a varicosity at one smooth muscle cell diameter (4 μm) below the surface gives a recorded current at the surface which is about 25% of that due to a varicosity at the surface (figure 7*d*).

(*d*) *Changes in the polarity of single excitatory junction potentials in the muscle syncytium*

The position of the varicosity with respect to the recording electrode determines the polarity of the EJC. However, a reversal of polarity sometimes occurs during single EJCs. One way in which this could arise relates to the fact that the timecourse of the exponential decline in the EJC, which is probably determined by the kinetics of interaction between the transmitter and the underlying receptors, varies by about 30%. If two surface varicosities which have different timecourse EJCs secrete at the same time, and one of these is at a site just within the electrode and the other just outside, then a reversal can occur during the EJC, as shown in figure 8*a*. A longer timecourse EJC generated outside the electrode can reverse the shorter timecourse EJC generated within the electrode. However, it

PHILOSOPHICAL TRANSACTIONS OF THE ROYAL SOCIETY B BIOLOGICAL SCIENCES

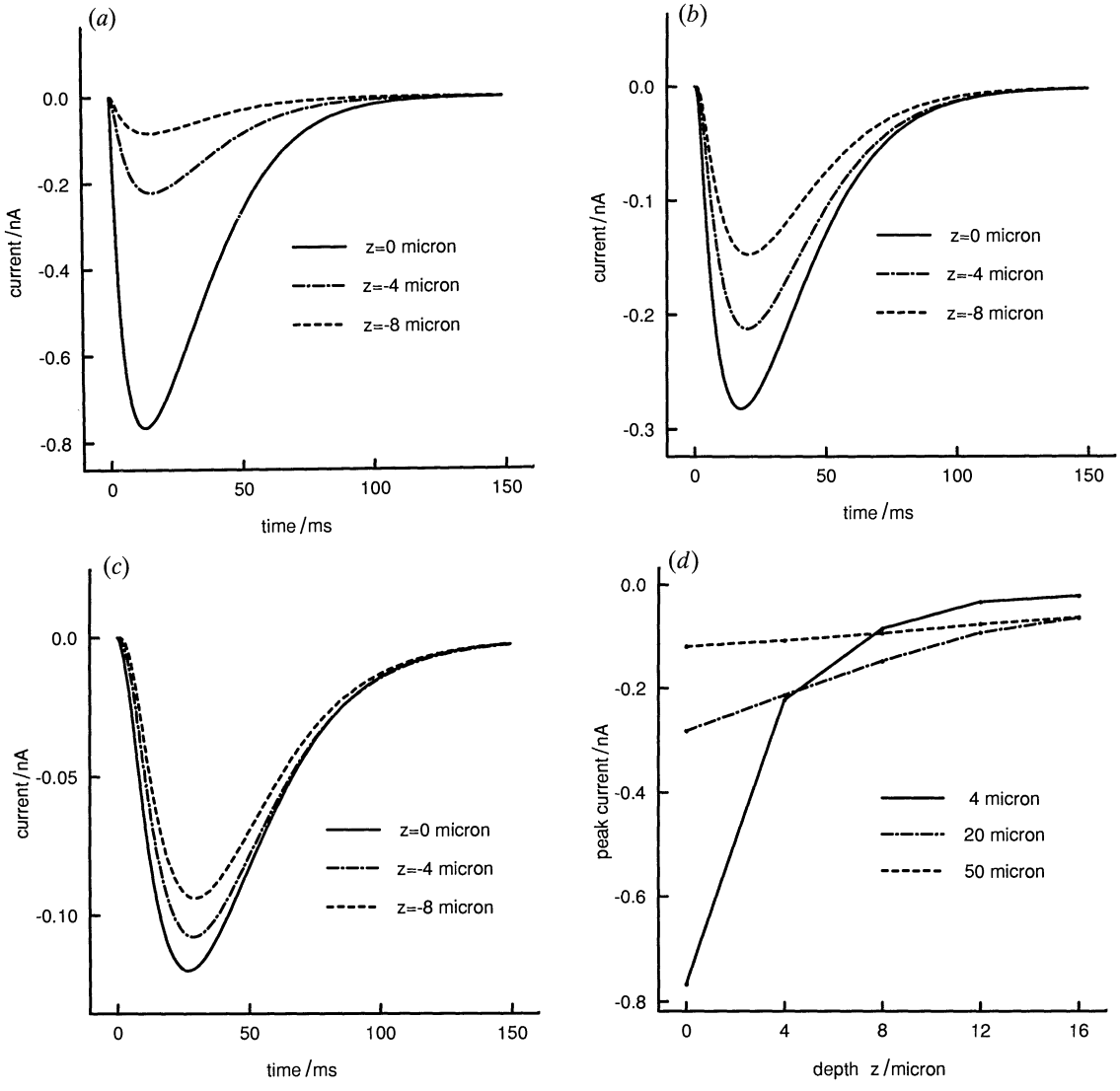

Figure 7. Changes in the amplitudes of the EJCs when the transmitter secretion occurs from varicosities at different depths below the centre of the extracellular recording electrode. The centre of the electrode is positioned at (0, 0, 0) and the varicosity is positioned at (0, 0, z). (*a*) Recordings with a 4 μm diameter electrode. Note the rapid decrease in amplitude of the EJC with increase in depth. (*b*) Recordings with a 20 μm diameter electrode. (*c*) Recordings with a 50 μm diameter electrode. Note the more gradual decrease in amplitude of the EJC with the increase in depth when using larger diameter electrodes in (*b*) and (*c*). (*d*) Changes in the peak amplitude of the EJC as the varicosity moves deeper into the tissue, for 4 μm, 20 μm and 50 μm electrodes. Note that the smaller diameter electrodes record much greater signals from a varicosity at the surface than from varicosities deeper in the tissue.

is possible to have a varicosity at the centre of a large-diameter electrode and another just outside, each generating an EJC with the same exponential decline, and collectively these give rise to a polarity reversal in the summed EJC (figure 8*b*).

Another way in which a reversal of polarity might occur during single EJC is related to the differences in delay between the arrival of the nerve impulse and secretion of transmitter from different sites in the syncytium. However, this latency can vary by only up to 4 ms, and this is insufficient to allow secretion at different sites to give polarity reversals in the EJC.

4. CONCLUSIONS: TESTS OF THE THEORY

Before comparing the theoretical results with experiment it should be emphasized that there are several shortcomings which preclude a detailed quantitative comparison. The most important of these are the assumption of zero extracellular current resulting in boundary condition (17), the assumption of equal anisotropy as given by equation (12), and the lumping of extended muscle cells into discrete points on a grid. All of these aspects require further detailed investigation. Nevertheless, the present theoretical model does contain enough of the real situation that a qualitative comparison with experiment is a valid undertaking.

The previous section shows that the amplitudes of EJCs recorded from a varicosity within the recording electrode and on the surface of the muscle depends on the position of the varicosity with respect to the centre of the electrode as well as on the diameter of the

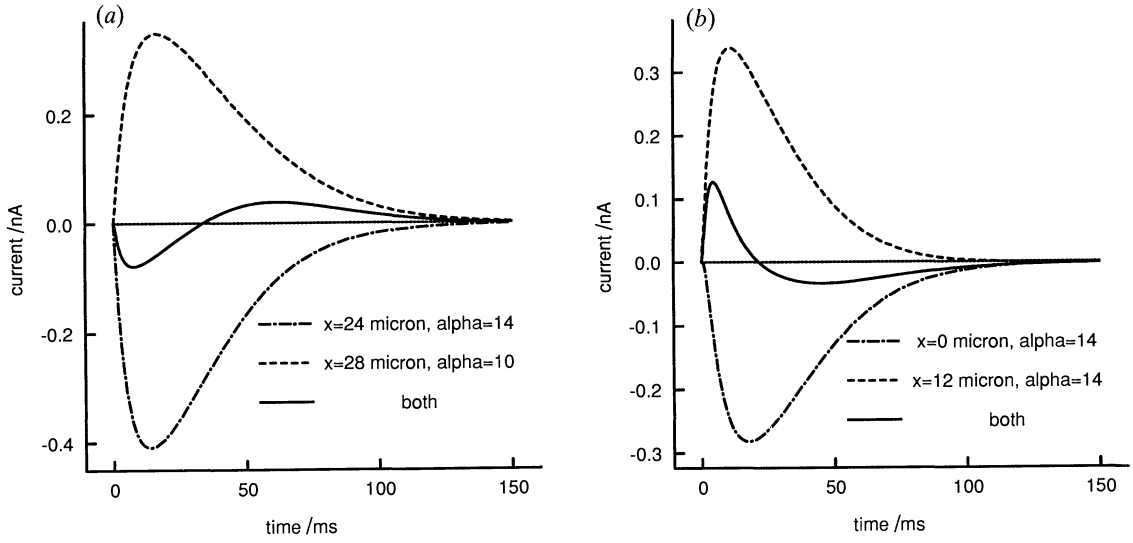

Figure 8. (*a*) Changes in polarity of current flow during a single EJC due to simultaneous secretion from two varicosities with different time constants, as measured by a 50 μm electrode. The first is inside the recording electrode at its edge $x = 24$ and has $\alpha = 14$; the second is outside the recording electrode at its edge $x = 28$ and has $\alpha = 10$. These time constants are at the maximum observed variation of 30%. The graph shows the EJCs due to each varicosity alone, and also the EJC due to the simultaneous secretion from both varicosities. (This is very close to the algebraic sum of the two individual EJCs, showing that interference effects are small in this case.) The reversal in the polarity of this recorded EJC is due to the disparity in the α values for the two varicosities. (*b*) Changes in polarity of current flow during a single EJC due to simultaneous secretion from two varicosities with the same time constants ($\alpha = 14$), as measured by a 20 μm electrode. The first is inside the recording electrode at its centre, not at the edge as in (*a*); the second is outside the recording electrode at its edge $x = 12$. The graph shows the EJCs due to each varicosity alone, and also the EJC due to both (which again is very close to the algebraic sum of the two currents).

electrode. Lavidis & Bennett (1992), using the mouse vas deferens, showed that smaller recording electrodes (20 μm diameter compared with 50 μm diameter) gave rise to larger EJCs (63 μV compared with 27 μV on average), in accord with the present theory. In addition, it was shown that larger EJCs were recorded if varicosities were found predominately towards the inside edge of the electrode (N. A. Lavidis & M. R. Bennett, personal observations), which again agrees with the present theory.

Varicosities deep within the tissue may produce EJCs recorded at the surface which are always smaller, but of comparable amplitude, than those generated by varicosities at the surface when electrodes greater than about 20 μm diameter are used (see figure 7*d*). Varicosities may occur one smooth muscle cell diameter (about 4 μm) from the surface, and these will contribute to the EJC recordings made with 20 μm diameter electrodes from surface varicosities (Lavidis & Bennett 1992). The statistical analysis of quantal secretion from such recordings is therefore suspect, due to the spatial decrement in the current recorded from varicosities at different positions within the electrode and in the depth of the tissue beneath the electrode. This problem is compounded if an attempt is made to correlate the binomial statistical parameter (n) with the number of visualized surface varicosities within the electrode, as it ignores contributions from varicosities deeper in the tissue. The only possible way to resolve this problem is to use small-diameter electrodes, about 4 μm in diameter, over single varicosities at the surface of the tissue. In this case, the EJCs generated outside the electrode are very small compared with those generated by a varicosity inside the electrode (see figure 5*d*). Lavidis & Bennett (1992) argued that varicosities 5 μm deep in the tissue beneath an electrode, that is, about one smooth muscle cell diameter away, could not contribute to the EJC; this is not the case, because the electrotonic decrement in the z-direction is slight for large-diameter electrodes (figure 7*d*).

The present theory shows that the skewed amplitude distributions of spontaneous EJCs recorded with large-diameter electrodes over large numbers of varicosities (see figure 2 in Åstrand & Stjärne (1988); figure 2 in Åstrand *et al.* (1988)) may arise from differences in the contributions which each of these makes to the recorded EJC, depending on their position within the electrode (see figures 5*d* and 7*d*). This interpretation is supported by the observation that small-diameter electrodes over single varicosities sometimes give Gaussian amplitude distributions (Lavidis & Bennett 1992).

Estimates of the probability of secretion have been made, in studies on the rat tail artery and guinea-pig vas deferens, by identifying evoked EJCs of like amplitude as originating from the same release site (Brock & Cunnane 1988). The present theory suggests that release sites at different positions within the electrode will indeed contribute very different-size EJCs (up to three-fold for the 50 μm electrodes used by Brock & Cunnane (1988); see figure 5*d*). As this variation is much greater than the variation in the EJC due to secretion from a single varicosity (see figure 8 in

Lavidis & Bennett (1992)), EJCs of similar amplitude may come from the same varicosity as suggested by Brock & Cunnane (1988).

EJCs of opposite polarity are often recorded with large-diameter electrodes. The positive EJCs are often of smaller amplitude than the negative ones (see, for example, figure 7 in Brock & Cunnane (1988)), but may be of the same size as the negative ones (see, for example, figure 2*a* in Stjärne & Stjärne (1989)). Both these observations are consistent with the results shown in figure 5*d*.

On some occasions a change in polarity may occur during a single EJC (see, for example, figure 6 in Åstrand & Stjärne (1988); figure 3*d* in Stjärne & Stjärne (1989)). This change in polarity sometimes occurs from a negative value, going to the peak of the EJC, followed by a positive tail during the declining phase. The present model shows that such EJCs can arise from differences in the timecourse of decline of EJCs, which can amount to about 30% (see figure 5*a* in Brock & Cunnane (1988)); if the current due to a positive EJC declines more slowly than that due to a negative EJC generated within the electrode, then a change in polarity of the recorded EJC can occur during its tail (see figure 8*a*). Changes in polarity of the EJC from a positive- to a negative-going component can arise when the current is generated by transmitter release on the outside edge of the recording electrode and simultaneously near the centre of the electrode (see figure 8*b*).

The present model provides an explanation for the properties of the synaptic potentials recorded with an extracellular electrode during transmitter release from varicosities in the smooth muscle syncytium. Further insight requires the development of a theory which treats a continuous rather than a discrete model of the syncytium (Schmitt 1969; Tung 1979), as well as more realistic boundary conditions at the recording electrode, and this work is in progress.

The authors thank Dr David Galloway for advice concerning numerical techniques. We also thank a referee for pointing out changes required to reflect the spatial structure of the smooth muscle cells. Support under ARC Grant AC9031997 is acknowledged.

REFERENCES

Åstrand, P., Brock, J.A. & Cunnane, T.C. 1988 Time course of transmitter action at the sympathetic neuroeffector junction in rodent vascular and non-vascular smooth muscle. *J. Physiol., Lond.* **401**, 657–670.

Åstrand, P. & Stjärne, L. 1988 On the secretory activity of single varicosities in the sympathetic nerves innervating the rat tail artery. *J. Physiol., Lond.* **409**, 207–220.

Bennett, M.R. 1967 The effect of intracellular current pulses in the smooth muscle cells of the guinea pig vas deferens at rest and during transmission. *J. gen. Physiol.* **50**, 2459–2475.

Bennett, M.R. 1972 *Autonomic neuromuscular transmission.* Monographs of the Physiological Society No. 30. Cambridge University Press.

Bennett, M.R. 1973 Structure and electrical properties of the autonomic neuromuscular junction. *Phil. Trans. R. Soc. Lond.* B **265**, 25–34.

Bennett, M.R. & Merrillees, N.C.R. 1966 Analysis of the transmission of excitation from autonomic nerves to smooth muscle. *J. Physiol., Lond.* **185**, 520–535.

Brock, J.A. & Cunnane, T.C. 1987 Relationship between the nerve action potential and transmitter release from sympathetic postganglionic nerve terminals. *Nature, Lond.* **326**, 605–607.

Brock, J.A. & Cunnane, T.C. 1988 Electrical activity at the sympathetic neuroeffector junction in the guinea-pig vas deferens. *J. Physiol., Lond.* **399**, 607–632.

Burnstock, G. & Holman, M.E. 1962 The transmission of excitation from autonomic nerves to smooth muscle. *J. Physiol., Lond.* **155**, 115–133.

Clerc, L. 1975 Directional differences in impulse speed in trabecular muscle from mammalian heart. *J. Physiol., Lond.* **255**, 335–346.

Cunnane, T.C. & Manchanda, R. 1990 On the factors which determine the time-courses of junction potentials in the guinea-pigs vas deferens. *Neuroscience* **37**, 507–516.

Hirst, G.D.S. & Neild, T.O. 1980 Some properties of spontaneous excitatory junction potentials recorded from arterioles of guinea-pigs. *J. Physiol., Lond.* **303**, 43–60.

Hodgkin, A.L. 1954 A note on conduction velocities. *J. Physiol., Lond.* **125**, 221–224.

Jack, J.J.B. & Redman, S.J. 1971 An electrical description of the motoneurone and its application to the analysis of synaptic potentials. *J. Physiol., Lond.* **215**, 321–352.

Lavidis, N.A. & Bennett, M.R. 1992 Probabilistic secretion of quanta from visualized sympathetic nerve varicosities in mouse vas deferens. *J. Physiol., Lond.* **454**, 9–26.

Purves, R.D. 1976 Current flow and potential in a three-dimensional syncytium. *J. theor. Biol.* **60**, 147–162.

Roberts, K.V. & Weiss, N.O. 1965 Convective difference schemes. *Math. Comp.* **20**, 272.

Schmitt, O.H. 1969 Biological information processing using the concept of interpenetrating domains. In *Information processing in the nervous system* (ed. K. N. Leibovic), pp. 325–332. New York: Springer.

Stjärne, L. & Stjärne, E. 1989 Basic features of an extracellular recording method to study secretion of a sympathetic co-transmitter, presumably ATP. *Acta physiol. scand.* **135**, 217–226.

Tomita, T. 1970 Electrical properties of mammalian smooth muscle. In *Smooth muscle* (ed. E. Bülbring, A. F. Bradling, A. W. Jones & T. Tomita), pp. 197–243. London: Arnold.

Tung, L. 1979 Three-dimensional cable theory: a bidomain model. *Biophys. J.* **25**, 214a.

Received 25 June 1992; accepted 18 May 1993

PHILOSOPHICAL TRANSACTIONS OF THE ROYAL SOCIETY B BIOLOGICAL SCIENCES